International Journal of Thermal Sciences 122 (2017) 39–52

Contents lists available at ScienceDirect

International Journal of Thermal Sciences

journal homepage: www.elsevier.com/locate/ijts

Experimental investigation on the thermal performance of a double pipe heat exchanger with segmental perforated baffles

M.R. Salem [a, *], M.K. Althafeeri [b], K.M. Elshazly [a], M.G. Higazy [a], M.F. Abdrabbo [a]

[a] Mechanical Engineering Department, Faculty of Engineering at Shoubra, Benha University, 108 Shoubra St., 11629 Cairo, Egypt
[b] Farwaniya Hospital, Ministry of Health, 86400 Farwaniya, Kuwait

ARTICLE INFO

Article history:
Received 12 July 2017
Received in revised form
9 August 2017
Accepted 11 August 2017

Keywords:
Perforated baffles
Heat exchanger
Passive technique
Heat transfer enhancement
Thermal performance
Friction
Experimental

ABSTRACT

This work experimentally investigates the characteristics of convective heat transfer and pressure drop of water flow in the annulus-side of horizontal double pipe heat exchangers. Twelve heat exchangers of counter-flow configurations are constructed with/without Single Segmental Perforated Baffles (SSPBs), which are fabricated with different holes spacing, void, cut, pitch ratios and inclination angle. The experiments are performed for annulus-side Reynolds number from 1380 to 5700, and for Prandtl number from 5.82 to 7.86. The results revealed that increasing SSPBs holes spacing and void ratios and inclination angle and decreasing SSPBs cut and pitch ratios increase the annulus average Nusselt number ($\overline{Nu}_{an}$) as well as friction factor (f_{an}). The thermal performance index (*TPI*) is calculated to compare the thermal performance of perforated baffled double pipe heat exchangers with un-baffled one. It is observed that increasing SSPBs holes spacing ratio and inclination angle, and decreasing SSPBs void ratio, cut ratio and pitch ratio enhances the thermal performance index. Finally, correlations for $\overline{Nu}_{an}$ in addition to f_{an} for concentric tube heat exchangers with SSPBs as a function of the investigated parameters are obtained.

1. Introduction

Numerous applications involve heat transfer processes, whereas conversion, utilization, and recovery of the energy in every industrial, commercial, and domestic application involve a heat transfer process. In most of these applications, heat is transferred through heat exchangers as in the chemical, electrical, power, petroleum, air-conditioning, refrigeration, cryogenic, heat recovery, and manufacturing industries. Therefore, enhancing the thermal performance of heat exchange affects directly on energy, material and cost savings. Consequently, improving the heat exchange above that in the usual or standard practice can significantly improve the thermal efficiency in such applications as well as the economics of their design and operation [1].

Double pipe heat exchangers are the simplest devices in which heat is transported from the hot fluid to the cold fluid through a separating cylindrical wall. They are primarily adapted to high temperature and high-pressure applications due to their small diameters. They are cheap, but the amount of space they occupy is relatively high compared to the other types [2].

To achieve the desired heat transfer rate in the given design and size of the heat exchanger at an economic pumping power, numerous techniques have been proposed. These enhancement techniques can be categorized as active and passive techniques. Furthermore, any two or more of these techniques (passive and/or active) may be employed simultaneously to obtain enhancement in heat transfer that is greater than that produced by only one technique itself. This simultaneous utilization is termed compound enhancement [3–6].

From the use and design point of view, active heat transfer enhancement techniques are more complex, as they require some external power to facilitate the desired flow modification and the associated improvement in the heat transfer rate. Thermal performance augmentation by this method can be attained by using mechanical aids, surface vibration, fluid vibration, electrostatic fields, injection, suction and jet impingement. While passive heat transfer enhancement techniques generally depend on the surface or geometrical modifications to the flow channel by incorporating inserts or additional devices. They provide higher heat transfer coefficients by disturbing or altering the existing flow behaviour except for extended surfaces. Passive techniques hold the advantage over the active techniques, as they do not need any direct input of external power. Heat transfer augmentation by this technique

* Corresponding author.
E-mail addresses: me_mohamedreda@yahoo.com, mohamed.abdelhamid@feng.bu.edu.eg (M.R. Salem).

http://dx.doi.org/10.1016/j.ijthermalsci.2017.08.008
1290-0729/

can be achieved by using treated surfaces, rough surfaces, extended surfaces, displaced enhancement devices, swirl flow devices, surface tension devices, coiled tubes and use of additives [3–6].

Baffles are one of the passive enhancement techniques, which are utilized to improve the thermal performance of heat exchangers that are widely used in various industries: chemical, biological, petrochemical, biomedical and others. The wide using of the baffles in heat exchangers is because they direct the shell-side fluid to move back and forth across the internal tube to increase the turbulence level and provide good mixing of the fluid layers. In addition, they eliminate dead spots and increase heat transfer rate. Furthermore, in shell and tube heat exchangers, they minimize tube-to-tube temperature differences, which reduces the thermal stresses. Additionally, they support the internal tubes during operation, which prevents bending and vibration. Due to the extensive use of the baffles, knowledge about the heat transfer and shell-side fluid flow characteristics are very important.

Ko and Anand [7] studied experimentally the heat transfer rate in heated rectangular channel subjected to constant heat flux with wall mounted perforated baffles in staggered arrangement. Compared to no baffles, the results showed a heat transfer enhancement of 300%, while this augmentation per unit increase in pumping power was less than one for the range of parameters studied in that work. Yang and Hwang [8] numerically presented predictions on the heat transfer and turbulent fluid flow characteristics in a rectangular channel with solid and perforated baffles mounted in a staggered way. The simulations indicated that the flow patterns around the porous- and solid-type baffles are completely different due to different transport phenomena and it significantly influences the local heat transfer coefficient distributions. Compared with the solid baffle, the perforated baffled channel has a lower friction factor due to less channel blockage. Dutta and Hossain [9] experimentally studied the local heat transfer and friction loss characteristics in a rectangular channel with inclined solid and perforated baffles. A combination of two baffles of same dimensions was used. The results demonstrated that the local Nusselt number and friction factor are strongly depended on the position, orientation, and geometry of the second baffle plate. Karwa et al. [10] studied the heat transfer and friction in rectangular ducts with solid and perforated baffles (with void ratio from 18.4% to 46.8%) attached to one of the broad walls. The baffled wall of the duct was subjected to constant heat flux while the remaining three walls were insulated. The results revealed that the baffles with the highest open area ratio give the best performance compared with the smooth duct at equal pumping power.

Balikowski and Mollendorf [11] experimentally and theoretically examined the thermal performance of a double pipe heat exchanger with employing two types of phase change materials in the annular region and water circulated in the internal pipe. The study was performed for smooth and spined finned annuli. The results revealed that the presence of spined fins in the phase change material accelerated charging and discharging. Targui and Kahalerras [12] carried out a numerical study of flow and heat transfer characteristics in a double pipe heat exchanger in which porous structures inserted into the annulus in two configurations: on the inner cylinder, and on both the cylinders in a staggered fashion. It was found that the highest heat transfer rates are obtained when the porous structures are attached in the last configuration. Nasiri et al. [13] presented an experimental study on the heat transfer performance of Al_2O_3/water and TiO_2/water nanofluids through an isothermal annular channel. The results illustrated that for specific Peclet number, Nusselt number of nanofluids is higher than that of the base fluid. Also, there was no significant difference in the enhancement for both nanofluids, which increased with the increase of nanoparticle concentration. Ary et al. [14] experimentally and numerically studied the influence of a number of tilted (5°) perforated baffles on the turbulent flow structures and heat transfer in the rectangular channel with different types of baffles. The results illustrated that the flow patterns around the holes are completely different with different numbers of holes and it meaningfully affects the local heat transfer, and two baffles provide greater heat transfer performances than a single baffle.

Targui and Kahalerras [15] numerically investigated the effect of the simultaneous use of perforated baffles and pulsating flow on a concentric tube heat exchanger performance. The effects of the amplitude and frequency of pulsation in addition to the baffles permeability on the flow pattern and the heat exchanger efficiency were analyzed. The results demonstrated that the addition of an oscillating component to the mean flow affects the flow pattern, and enhances the heat transfer in comparison to the steady non-pulsating flow. The highest heat exchanger performance was obtained when only the flow of the hot fluid is pulsating. Chamoli and Thakur [16] mathematically studied the performance of solar air heaters with V-down perforated baffles as roughness on the airflow side of the absorber plate. They indicated that the thermal and effective efficiencies differ only slightly at lower flow rates. In another work, Chamoli and Thakur [17] numerically investigated the effect of transverse perforated baffles attached to the heated wall of a rectangular duct on heat transfer and friction factor. They observed that installing perforated baffles enhances the heat transfer, while friction loss increases over a smooth surface. Sheikholeslami et al. [18,19] conducted experimental studies on friction loss and heat transfer enhancement in an air to water double pipe heat exchanger. Typical circular-ring and perforated circular-ring turbulators were studied. In their investigation, air flowed in the annular pipe. Experimental analysis was carried out for open area ratio; 0, 0.0208–0.0833, Reynolds number; 6000–12000 and pitch ratio; 1.83–5.83. The results showed that installing perforated circular-rings decreased the heat transfer enhancement compared with the circular rings because of reduction of intersection angle between the velocity and the temperature field. In addition, the thermal performance increased with the increase in number of rings but it decreased with increase of Reynolds number and pitch ratio. Sahel et al. [20] numerically examined the performance of SSPB (having a row of four holes placed at three different positions) aiming to enhance the heat transfer phenomenon in a rectangular channel. They observed that there was an enhancement in the heat transfer rate from 2% to 65% compared with the simple baffle. Kumar and Kim [21] numerically presented heat transfer and fluid flow characteristics in a solar air heater channel with multi V-type perforated baffles. The baffle height ratio, pitch ratio, baffle-hole position ratio, inclination angle, and baffle void ratio were 0.6, 8.0, 0.42, 60°, and 12%, respectively. Multi V-type perforated baffles were shown to have better thermal performance as compared to other baffle shapes in a rectangular passage.

El-Maghlany et al. [22] experimentally tested the effect of a compound heat transfer enhancement technique on the thermal performance of a horizontal double tube heat exchanger. Cu/water nanofluid (volume fractions of 0–3%) was employed in the annulus-side, while the inner tube was rotated with speed from 0 to 500 rpm. The results demonstrated a significant augmentation in the heat transfer rate and heat exchanger effectiveness and number of transfer units. Moreover, the use of the nanofluid has a little penalty in pressure drop in compared with the inner tube rotation. Sheikholeslami and Ganji [23] presented an experimental and numerical investigation on convective heat transfer and friction loss in a double pipe heat exchanger employed with perforated turbulators in annulus region. Effect of turbulators pitch ratio, open area ratio and Reynolds number (6000–12000) were considered.

The results revealed that thermal performance enhances with increasing open area ratio, while temperature gradient reduces with augmenting of pitch ratio. In another work, Sheikholeslami and Ganji [24] experimentally and numerically investigated the effect of perforated and typical helical fin on hydrothermal treatment in a water to air heat exchanger. Effects of pitch ratio, Reynolds number and open area ratio are examined. Empirical correlations for thermal performance, friction factor and Nusselt number were obtained. Results demonstrated that higher open area ratio provides greater thermal performance. In addition, the temperature gradient attenuates with enhancing of open area ratio. Sheikholeslami and Ganji [25] experimentally and numerically performed same work for square and circular section discontinuous helical fins. Results showed that the use of square section helical fins provides a higher heat transfer enhancement. Arzani et al. [26] experimentally investigated the heat transfer characteristics and pressure drop of multiwall carbon nanotube-water based nanofluid (mass fractions of 0–0.1%) in the annular side of a horizontal double pipe heat exchanger. Annular heat exchanger showed a significant increase in heat transfer rate with insignificant increase in pumping power for annulus Reynolds number range of 2420–6820. Kumar et al. [27] experimentally examined the effect of circular perforated ring insert on the thermal performance of the heat exchanger for Reynolds number range of 6500–23000. The test section was heated with a constant heat flux of 1000 W/m^2. It was found that there is a significant increase in both heat transfer and pressure drop, with a maximum thermal performance index of 1.47.

Chamoli et al. [28] successfully employed Taguchi-grey analysis method to investigate the geometric and flow parameters on the performance of a double pipe heat exchanger with perforated disk inserts. They evaluated the parametric influence on the system performance and then they conducted experimental runs using the obtained optimal design condition, to validate the improvement in the performance. The study illustrated the feasibility of the Taguchi-grey approach for predicting performance, optimization and improving the design of these heat exchangers. Chamoli et al. [29] experimentally investigated the thermal characteristic of a turbulent flow through an iso-fluxed circular tube fitted with a novel type of perforated vortex generator inserts for Reynolds number range of 3000–21000. The perforated vortex generators were cut from a cone into two identical shapes and attached to the opposite sides of a central rod at specific axial positions. The results showed a maximum thermal performance index of 1.65. The authors proposed correlations of Nusselt number and friction factor. In another research, Chamoli et al. [30] experimentally reported a multi-objective optimization of a heat exchanger tube fitted with compound insert geometries using response surface methodology. It was concluded that the acquired Pareto optimal configurations provide principal understanding into the design parameters and allow autonomy of selection among the optimal solutions. Sheikholeslami and Bhatti [31] numerically investigated the characteristics of forced convective heat transfer of nanofluids in a porous semi-annulus in presence of uniform magnetic field. Results illustrated that velocity of nanofluid augments with the increase of Darcy and Reynolds numbers. Moreover, platelet shape provided the highest rate of heat transfer. Finally, Nusselt number enhanced with increase of nanofluid fraction, Darcy and Reynolds numbers while it reduced with the increase of Lorentz forces. In another numerical investigation, Sheikholeslami and Shehzad [32], studied Magnetohydrodynamic CuO-water nanofluid flow in a porous iso-fluxed semi annulus. Here, they tested the effect of the radius of the inner cylinder, CuO nanoparticles concentration, Hartmann and Rayleigh numbers for the porous medium. A formula for the average Nusselt number was presented. Results demonstrated that heat transfer enhancement decreased with rising of buoyancy forces, and the influence of adding nanoparticle augmented with increase of Lorentz forces. Finally, increasing Hartmann number leads to a reduction in temperature gradient.

In Sheikholeslami [33], a mesoscopic method was applied to study nanofluid forced convection in three-dimensional porous geometry in existence of uniform Lorentz forces. The results showed that Lorentz force decreased convection heat transfer. In addition, the temperature gradient and velocity over the hot surface increased with rising of Reynolds number, Darcy number, nanoparticles concentration but it reduced with augmenting of Hartmann number. Al-Kayiem et al. [34] presented experimental results on improving the heat transfer using energy promoters have ribs shape with rectangular cross section, installed on the inner surface of the annulus for Reynolds number range of 2900–21000. The results showed that enhancement in the heat transfer was combined with a penalty in the pressure drop. Maakoul et al. [35] numerically investigated the thermal performance of a helically baffled double pipe heat exchanger. The results revealed that heat transfer performance and annulus pressure drop increased compared to the simple heat exchanger, and they are increasing functions of baffle spacing and Reynolds number.

The aforementioned literature survey indicates that the majority of studies performed on perforated baffles that were mounted inside rectangular channels. In addition, it is found that the thermal performance due to using the perforated baffles is more than that of using solid baffles. Despite the importance of double pipe heat exchangers, but it is found that there has not been any investigations on enhancing the heat transfer in their annulus with SSPBs. Therefore, the objective of the present work is to investigate experimentally the convective heat transfer and pressure drop in an annulus with perforated SSPBs aligned along the inner heated tube surface, using water as a working fluid. The experimental measurements are performed to investigate the effect of the baffle open area ratio, holes spacing ratio, baffles cut and pitch ratios, in addition to their inclination angles at a wide range of annulus-side operating conditions.

2. Experimental apparatus

The apparatus used in this study comprises hot and cold loops. The hot circuit consists of a heating unit, pump, valves, flow meter, straight tube and the connecting pipes. The cold circuit consists of cooling unit, pump, flow meter, valves, annular pipe with/without SSPBs and the connecting pipes. Fig. 1 is a schematic diagram of the experimental setup. In addition, Fig. 2 represents photos for the present setup and the test section.

The heating and cooling units are made of 50 liters stainless steel (2 mm wall thickness) cylindrical tank for each. Each tank is installed inside 2 mm thick galvanized steel tanks with 2 cm gap, which is filled with spray foam insulation to minimize the heat gain/loss from/to the atmosphere. For the heating unit, an electric heater (has a maximum power rating of 6 kW) is fixed horizontally on the bottom of the heating tank and performed the function of heating the water to the required temperature. On the other side, the heat is removed from the water in the cooling tank by two cooling units of 10.5 kW cooling capacity. Sometimes, the two units operate in series, and in other times, in a parallel manner to prevent thermal overloads.

The operations of the electric heater and the cooling units are based on pre-adjusted digital thermostats, which are used to keep constant temperatures of the liquids directed to the heat exchanger, whether for the tube-side or the annulus-side. Additionally, there are four ports in each tank; two of them are on the top covers of the tanks, represent the inlet ports from the heat exchanger and from the by-pass line. The other two ports are on the bottom, which

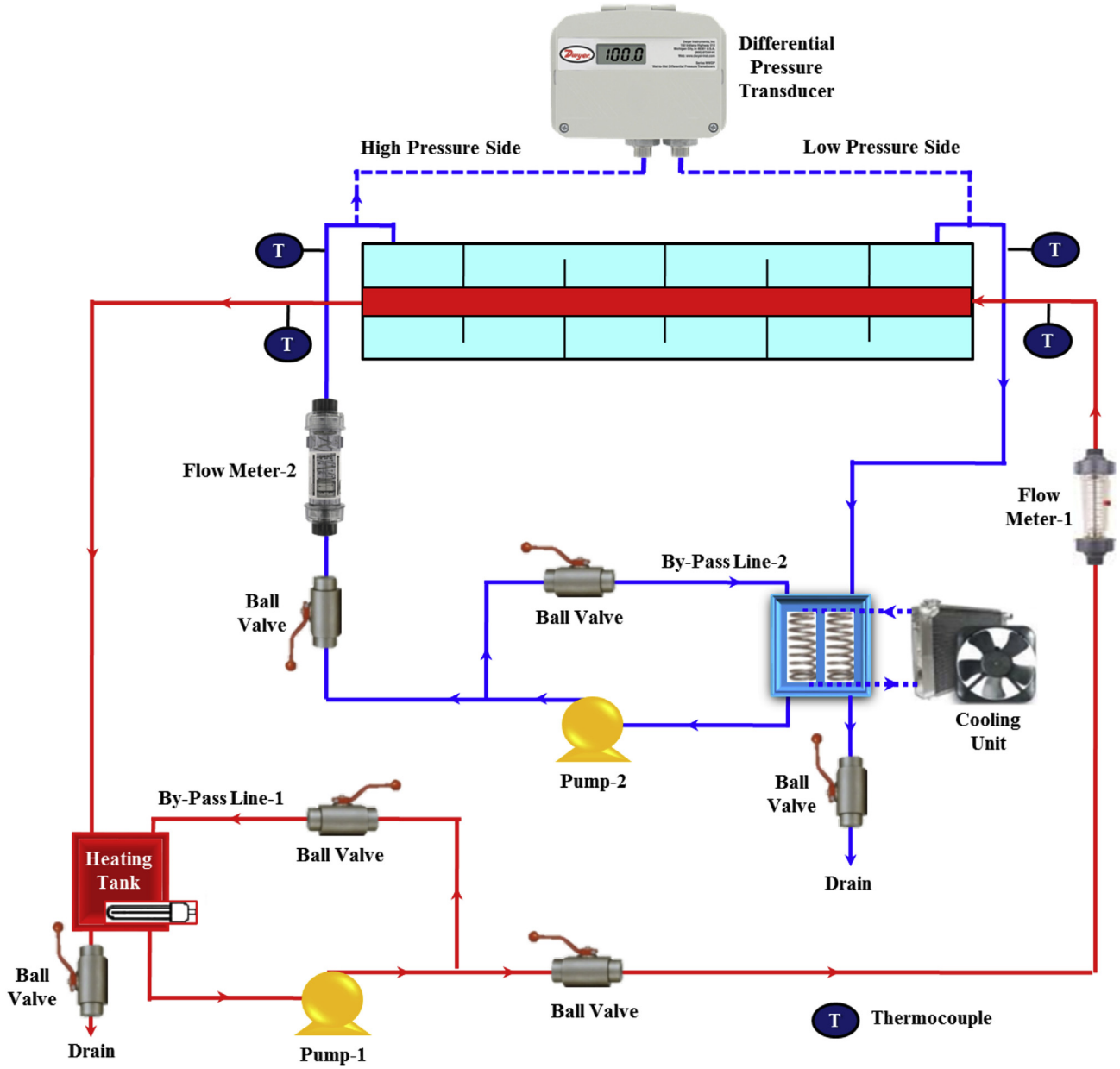

Fig. 1. Schematic of the experimental setup.

represent the exit ports to the drain and to the pump.

Two rotameters (1.7–18 l/min) are used to measure the volume flow rates of the two main loops fluids. The two flow meters have been calibrated by calculating the time required to fill a vessel with 20-litre capacity. Four K-type thermocouples (wires of 0.1 mm diameter) are directly inserted into the flow streams, at approximately 5 cm from the heat exchanger ports, to measure the inlet and exit temperatures of the annulus and internal tube fluids.

The thermocouples are connected via switching box to a digital thermometer indicator with a resolution of 0.1 °C to display the measured temperatures. All thermocouples are calibrated in the laboratory against a mercury-in-glass thermometer, which could be accurately read to ± 0.5 °C. A digital differential pressure transducer is employed for measuring the pressure drop of water between the annulus inlet and outlet. Two identical 1.5 hp power rating centrifugal pumps; are used; pump-1 is used to circulate the heating water on the internal tube-side, while pump-2 is used to circulate the cooling water on the annulus-side. Flexible nylon and Polyvinyl Chloride (PVC) tubing are used for all connections.

Twelve concentric tube heat exchangers of counter-flow configurations are constructed; one is without any baffles, while eleven heat exchangers are fabricated with different SSPBs holes spacing ratio (Ψ), void ratio (ϕ), cut ratio (δ), pitch ratio (λ) and inclination angle (θ). Schematic diagrams of the SSPBs is shown in Fig. 3 and the characteristic dimensions of the different configurations are revealed in Table 1. The SSPBs are formed from 0.6 mm thick copper sheet and a laser is used during cutting and drilling process. All baffles have a circular shape of the same diameter of the heat exchanger annular pipe; 50.8 mm except the inclined SSPBs which have a parabolic shape to keep the same cut ratio.

The annular pipe of the heat exchangers is made up of PVC tubes of 50.8 mm internal diameter and 4 mm wall thickness. Their ends are closed using PVC caps and adhesives to prevent any leakage. The internal tube of all exchangers is a copper tube of 26 mm

Fig. 2. Photos for the present experimental setup and the test section; (a) The test section (concentric tube heat exchanger with SSPBs), (b) Experimental setup.

internal diameter and 28 mm external diameter. The length of all heat exchangers annular pipes and their internal tube is 1200 mm. The outer surface of all annular pipes is thermally isolated with thick insulation consisting of layers of ceramic fiber, asbestos rope, and glass wool.

3. Experimental procedures

The experimental procedures are initiated after assembling the following equipments: the concentric tube heat exchanger, heating and cooling units, pumps, piping, flow meters, thermocouples and the differential pressure transducer. The thermocouples are attached at the inlet and outlet of the annulus and internal-tube sides. The first step to collect the data from the system is to fill the heating and cooling tanks with water from the local water supply. Then, the heater, the cooling unit and the pumps are operated. The inlet temperatures of the fluids in both sides are adjusted by regulating the temperatures of the heating and cooling tanks through their thermostats. The flow rates are adjusted through the flow meters and the installed valves, which are regulated to obtain the required flow rates in the primary lines and the remainder is bypassed to the reservoirs. The range of the operating conditions is given in Table 2.

Totally, a series of 252 experiments are carried out on the twelve heat exchangers; 231 runs for the heat exchangers with SSPBs and 21 runs for the un-baffled one. During the test operation, the steady-state condition is conducted when a maximum variation of 0.5°C for each thermocouple reading within 20 min is recorded. Moreover, it is considered to be achieved when the stable fluid inlet and outlet temperatures are obtained; variation of inlet and outlet temperatures of the two streams are within 0.2°C during a minute period before each measurement is taken.

4. Data reduction

Excel sheets are prepared to process the experimental data for the heat transfer coefficients and pressure drop. It should be noted that for all calculations, the thermophysical properties of the water in the annulus and internal tube are calculated at the bulk temperatures, $T_{an,\,m}$ and $T_{t,\,m}$, respectively, and are evaluated from Ralph [36].

$$T_{an,\,m} = (T_{an,\,i} + T_{an,\,o})/2 \tag{1}$$

$$T_{t,\,m} = (T_{t,\,i} + T_{t,\,o})/2 \tag{2}$$

4.1. Heat transfer calculations

The primary measurements in heat transfer calculations consist of six variables, namely the flow rates and the inlet and outlet temperatures of both streams of the heat exchanger. The heat transfer rates on the inner tube and annulus sides (Q_t and Q_{an}) are calculated by;

$$Q_t = \dot{m}_t Cp_t (T_{t,\,i} - T_{t,\,o}) \tag{3}$$

$$Q_{an} = \dot{m}_{an} Cp_{an} (T_{an,\,o} - T_{an,\,i}) \tag{4}$$

Assuming that the measurements are sufficiently accurate without heat gain or loss, there is an energy balance between the two streams ($Q_t = Q_{an}$). While in the real experiments, there would always be some discrepancy between the two rates. Therefore, the arithmetical mean of the two, Q_{ave}, can be used as the heat load of the exchanger. For all experimental tests, the heating and cooling loads calculated from the hot and cold sides did not differ by more than ±5.1%.

$$Q_{ave} = \frac{|Q_t| + |Q_{an}|}{2} \tag{5}$$

The overall thermal conductance is calculated from this heat load, the temperature data and flow rates using Eq. (6);

$$U_i A_{t,\,i} = \frac{Q_{ave}}{\Delta T_{L.M}} \tag{6}$$

$$\Delta T_{L.M} = \frac{(\Delta T_i - \Delta T_o)}{ln\left[\frac{\Delta T_i}{\Delta T_o}\right]} = \frac{(T_{t,\,i} - T_{an,\,o}) - (T_{t,\,o} - T_{an,\,i})}{ln\left[\frac{T_{t,\,i} - T_{an,\,o}}{T_{t,\,o} - T_{an,\,i}}\right]} \tag{7}$$

Neglecting the thermal resistances of the tube wall and fouling, the overall thermal conductance can be expressed in terms of the thermal resistances.

$$\frac{1}{U_i A_{t,\,i}} = \frac{1}{\overline{h}_{an} A_{t,\,o}} + \frac{1}{\overline{h}_t A_{t,\,i}} \tag{8}$$

The water flow in the inner tube is turbulent and fully developed where the ratio between the tube-length to the inner diameter is 46.2, which is more than 10. The average Nusselt number for the tube-side fluid, $\overline{Nu}_t$, can be calculated using Dittus-Boelter [37] correlation for fully developed turbulent flow, Eq. (9),

$$\overline{Nu}_t = 0.023\, Re_t^{0.8}\, Pr_t^{0.3} \tag{9}$$

Then the average heat transfer coefficient for the tube-side fluid, $\overline{h}_t$, can be obtained as follows;

$$\overline{h}_t = \frac{\overline{Nu}_t . k_t}{d_{t,\,i}} \tag{10}$$

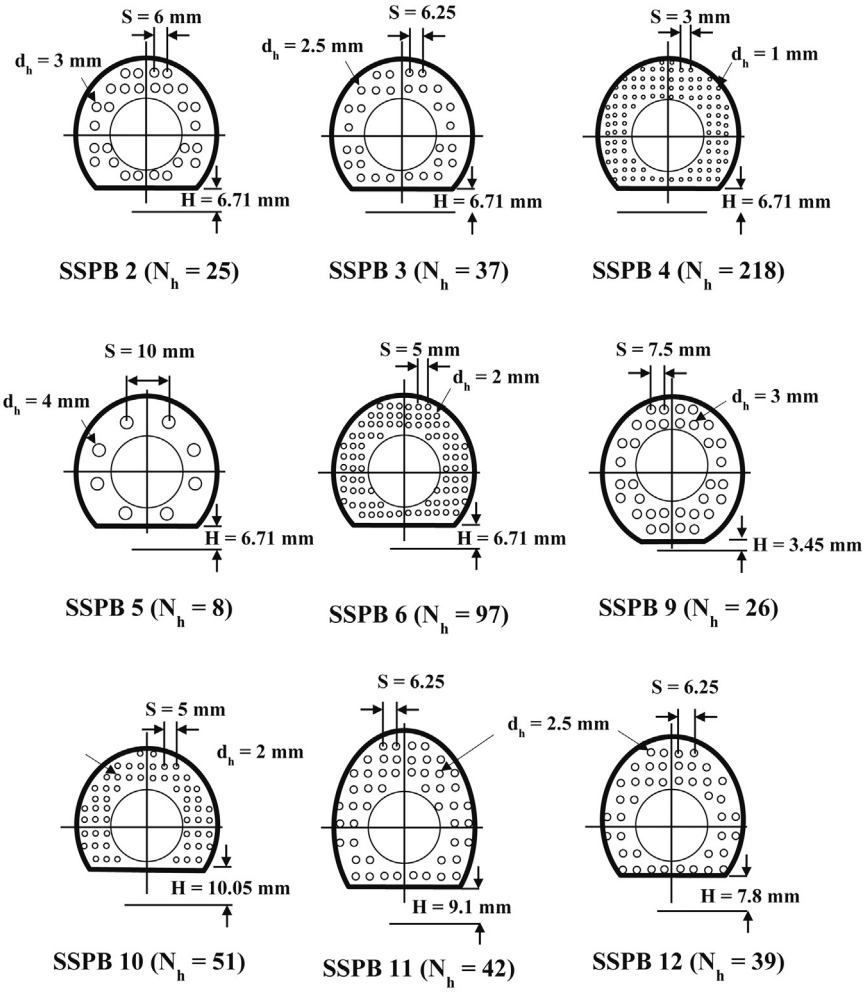

Fig. 3. Schematic diagrams of the SSPBs.

The average Nusselt number for the annulus-side fluid, $\overline{Nu}_{an}$, can be obtained as follows;

$$\overline{Nu}_{an} = \frac{\overline{h}_{an}\, d_{an,\,h}}{k_{an}} \tag{11}$$

Where $d_{an,\,h}$ is the hydraulic diameter of the annulus, $d_{an,\,h} = d_{an,i} - d_{t,o}$. Tube and annulus Reynolds numbers can be written as follows;

$$Re_t = \frac{4\dot{m}_t}{\pi d_{t,\,i}\mu_t} \tag{12}$$

$$Re_{an} = \frac{4\dot{m}_{an}}{\pi d_{an,\,h}\mu_{an}} \tag{13}$$

4.2. Friction factor calculation

In the present study, the measurement of the friction factor is conducted at the same time as the heat transfer measurements to show the effect of using the SSPBs in the annulus of the heat exchanger at different operating conditions. The Fanning friction factor for the fluid in circulation inside the annulus side is calculated with the following equation;

$$f_{an} = \frac{\Delta P_{an}\, d_{an,\,h}}{2L_{an}\,\rho_{an} u_{an}^2} \tag{14}$$

$$u_{an} = \frac{\dot{V}_{an}}{\frac{\pi}{4}\left(d_{an,\,i}^2 - d_{t,\,o}^2\right)} \tag{15}$$

5. Uncertainty analyses

In general, the accuracy of the experimental results depends on the accuracy of the individual measuring instruments and techniques. It should be noted that according to the manufacturer, uncertainty (ω) in the internal tube outer and inner diameters, and in all dimensions of baffles; diameter, window height, holes diameter and spacing is ±0.05 mm. The uncertainty in the measured annulus diameters and lengths, in addition to the pitch between the SSPBs, is ±0.5 mm. The uncertainty of the parameters is calculated based upon the root sum square combination of the effects of each of the individual inputs as introduced by Kline and McClintock [38]. For all experimental runs, the maximum uncertainties in main parameters are summarized in Table 3. For the estimated uncertainties in the other variables and parameters used

Table 1
Characteristic dimensions of the used perforated baffles.

SSPB no.	H (mm)	d_h (mm)	N_h	S (mm)	Ψ	ϕ (%)	p_b (mm)	λ (%)	δ (%)	N_b	θ
1	No baffles										
2	6.71	3.0	25	6.00	2	12.14	200	8.77	13.2	5	90°
3		2.5	37	6.25	2.5						
4		1.0	218	3.00	3						
5		4.0	8	10.0	2.5	6.72					
3		2.5	37	6.25		12.14					
6		2.0	97	5.00		20.4					
7		2.5	37	6.25		12.14	300	13.16		3	
3							200	8.77		5	
8							150	6.58		7	
9	3.45	3	26	7.50			200	8.77	6.6	5	
3	6.71	2.5	37	6.25					13.2		
10	10.05	2	51	5.00					19.8		
11	9.1	2.5	42	6.25					13.2		45°
12	7.8		39								60°
3	6.71		37								90°

in the present study, additional information is given in Appendix A.

6. Apparatus validation and data verification

Using the aforementioned experimental procedures and analysis methods, the validation of the methodologies in determining the heat transfer coefficients and friction factors is done by taking measurements of the flow in the annulus and comparing it with established heat transfer and friction factor correlations. For heat transfer and friction factor calculations, the experimental procedures are validated by comparing the results of $\overline{Nu}_{an}$ for the water flowing through the annulus with $\overline{Nu}_{an}$ for turbulent flow developed by Gnielinski [39], Eq. (16).

$$\overline{Nu}_{an} = \frac{\frac{f_{an}}{2}(Re_{an} - 1000)Pr_{an}}{1 + 12.7\sqrt{\frac{f_{an}}{2}}\left(Pr_{an}^{2/3} - 1\right)}\left[1 + \left(\frac{d_{an,\,h}}{L_{an}}\right)^{2/3}\right] \tag{16}$$

The Fanning friction factor in Eq. (16) is calculated according to Filonenko [40], through Eq. (17), which is also used for comparing the results of f_{an} for the water flowing through the annulus.

$$f_{an} = 0.25(1.82 \log Re_{an} - 1.64)^{-2} \tag{17}$$

The results of these comparisons are shown in Figs. 4 and 5. The range of the operating conditions during validation is given in Table 4. It is indicated that the experimental results for both heat transfer and friction factor calculations are in good agreement with previous studies with an average deviation of 10.1% and 3.1% for annulus average Nusselt number and Fanning friction factor, respectively. This good agreement in comparisons reveals the accuracy of the experimental setup and measurement technique.

7. Results and discussions

Totally, a series of 252 experiments are carried out on the twelve heat exchangers; 21 runs for the case of no baffles and 231 runs for the heat exchangers with SSPBs, which are constructed with different cut, void, spacing, pitch ratios and inclination angles. These configurations are tested at different flow rates (6.01–18.26 l/min) and inlet temperatures (15, 20 and 25 °C) for the annulus side of heat exchanger. All specifications and operating parameters are revealed in Table 2. The corresponding dimensionless are $1380 \le Re_{an} \le 5700$, $5.82 \le Pr_{an} \le 7.86$, $2 \le \Psi \le 3$, $6.72\% \le \phi \le 20.4\%$, $6.6\% \le \delta \le 19.8\%$, $6.58\% \le \lambda \le 13.16\%$ and $45° \le \theta \le 90°$. Heat transfer results in terms of annulus-side average Nusselt number and overall heat transfer coefficient in addition to the annulus-side Fanning friction are presented in the following subsections for the different governing parameters at $T_{an,\,i} = 20$°C as a sample of the results.

Table 2
Range of fluids operating conditions.

Parameters/operating conditions	Range or value
Annulus-side water flow rate, l/min	6.02–18.36 ($1380 \le Re_{an} \le 5700$)
Annulus-side water inlet temperature, °C	15, 20, 25 ($5.82 \le Pr_{an} \le 7.86$)
Tube-side water flow rate, l/min	8.06
Tube-side water inlet temperature, °C	50

Table 3
Maximum uncertainties in the main parameters.

Parameter	Uncertainty (%)
Annulus-side Reynolds number	±2.79
Annulus-side average Nusselt number	±6.74
Annulus-side average heat transfer coefficient	±6.35
Tube-side Reynolds number	±1.67
Tube-side average Nusselt number	±1.68
Tube-side average heat transfer coefficient	±1.68
Overall heat transfer coefficient	±2.86
Annulus-side Fanning friction factor	±4.48

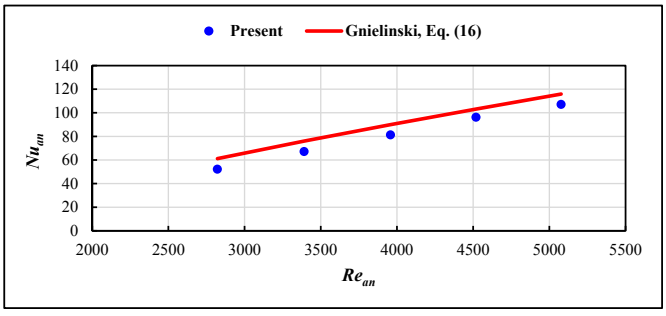

Fig. 4. Validation of the experimental average Nusselt number for the annulus side.

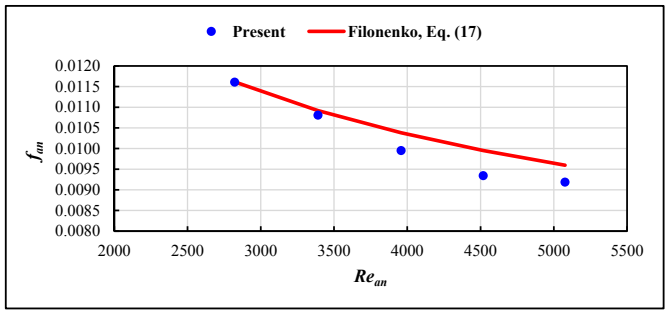

Fig. 5. Validation of the experimental Fanning friction factor for the annulus side.

7.1. Influence of SSPBs holes spacing ratio

In this analysis, four heat exchangers (SSPBs no. 1, 2, 3 and 4) are considered. Five SSPBs are inserted in the baffled heat exchangers with same void ratio ($\phi = 12.14\%$), same pitch ratio ($\lambda = 8.77$), same cut ratio ($\delta = 13.2\%$), same inclination angle ($\theta = 90^{\circ}$) while the holes spacing ratio ranges from 2 to 3.

Fig. 6 illustrates the effect of SSPBs spacing ratio on the annulus-average Nusselt number, overall heat transfer coefficient and annulus-side Fanning friction factor. It is revealed that increasing Ψ increases both $\overline{Nu}_{an}$, U_i and f_{an}. Compared with no baffles for all tested annulus-side operating conditions, the average increase in the annulus-average Nusselt number is of 34.8%–56.4%, and the average increase in the overall heat transfer coefficient is of 14%–21% and the average increase in the annulus-side friction factor is of 26.3%–39.2% when Ψ increases from 2 to 3. This may be due to increasing Ψ is accompanied by increasing number of the holes in the baffle with decreasing their diameters, for same baffle diameter and other geometrical parameters. This increases the throttling for the annulus flow and produces better impingement. This breaks the fluid boundary layer and creates a significant enhancement of heat transfer in addition to a significant increase in the pressure drop.

7.2. Influence of SSPBs void ratio

In this analysis, also four heat exchangers (SSPBs no. 1, 5, 3 and 6) are considered. Five SSPBs are inserted in the baffled heat exchangers with same holes spacing ratio ($\Psi = 2.5$), same pitch ratio ($\lambda = 8.77$), same cut ratio ($\delta = 13.2\%$), same inclination angle ($\theta = 90^{\circ}$) while the void ratio ranges from 6.72% to 20.4%.

Fig. 7 illustrates the obtained results. It is clear that increasing ϕ increases $\overline{Nu}_{an}$, U_i and f_{an}. Compared with no baffles for all tested annulus-side operating conditions, the average increase in the annulus-average Nusselt number is of 23.3%–73.8%, and the average increase in the overall heat transfer coefficient is of 9.9%–25.5% and the average increase in the annulus-side friction factor is of 18.1%–51% when ϕ increases from 6.72% to 20.4%. This can be attributed to increasing ϕ requires also increasing number of the holes in the baffle with decreasing their diameters, for same baffle diameter and other geometrical parameters, which produces the same effect of SSPBs spacing ratio, where they create a flow blockage and increase the flow velocity.

Table 4
Validation operating conditions.

Parameter	Operating conditions
Annulus-side water flow rate, l/min	10.09–18.26 ($2820 \leq Re_{an} \leq 5080$)
Annulus-side inlet temperature, °C	$Pr_{an} \cong 6.76$
Tube-side water flow rate, l/min	8.06
Tube-side inlet temperature, °C	50

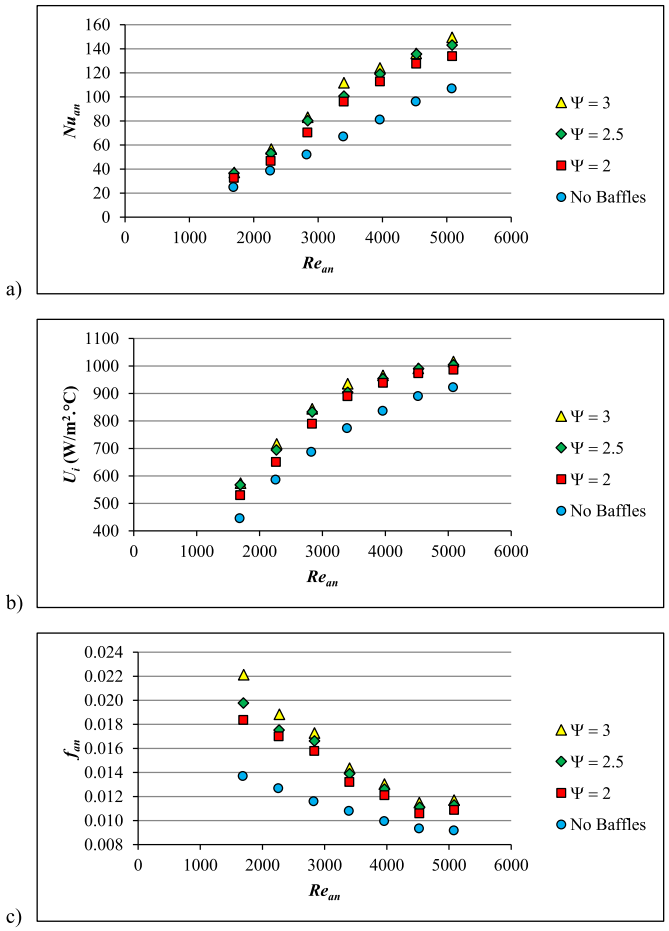

Fig. 6. Influence of SSPBs holes spacing ratio at different annulus Reynolds numbers; (a) $\overline{Nu}_{an}$, (b) U_i, (c) f_{an}.

7.3. Influence of SSPBs cut ratio

In this analysis, also four heat exchangers (SSPBs no. 1, 7, 3 and 8) are considered. Five SSPBs are inserted in the baffled heat exchangers with same holes spacing ratio ($\Psi = 2.5$), same void ratio ($\phi = 12.14\%$), same pitch ratio ($\lambda = 8.77$), same inclination angle ($\theta = 90^{\circ}$) while the cut ratio ranges from 6.6% to 19.8%.

From Fig. 8, it is obvious that decreasing δ increases $\overline{Nu}_{an}$, U_i and f_{an}. Compared with no baffles for all studied annulus-side operating conditions, the average increase in the annulus-average Nusselt number is of 16.8%–94.6%, and the average increase in the overall heat transfer coefficient is of 7.8%–30.7% and the average increase in the annulus-side friction factor is of 12.3%–59.2% when δ decreases from 19.8 to 6.6%. This is due to decreasing δ increases the throttling for the annulus flow and produces better impingement that creates a significant enhancement of heat transfer in addition to a remarkable increase in the pressure drop.

7.4. Influence of SSPBs pitch ratio

In this analysis, also four heat exchangers (SSPBs no. 1, 9, 3 and 10) are considered. The SSPBs are inserted in the baffled heat exchangers with same holes spacing ratio ($\Psi = 2.5$), same void ratio ($\phi = 12.14\%$), same cut ratio ($\delta = 13.2\%$), same inclination angle ($\theta = 90^{\circ}$) while the pitch ratio varies; 6.58%, 8.77% and 13.16%, and

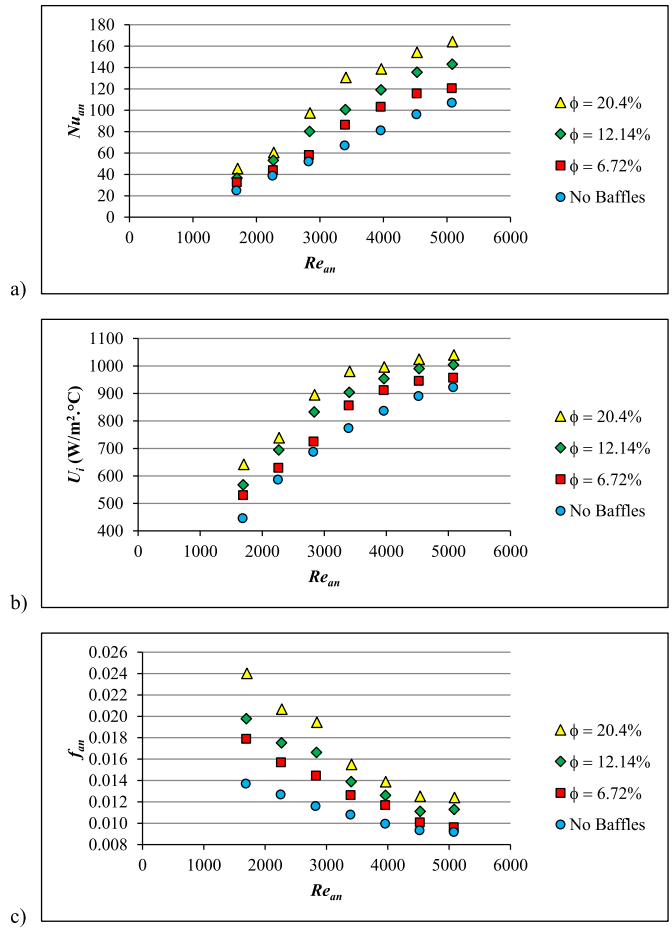

Fig. 7. Influence of SSPBs void ratio at different annulus Reynolds numbers; (a) $\overline{Nu}_{an}$, (b) U_i, (c) f_{an}.

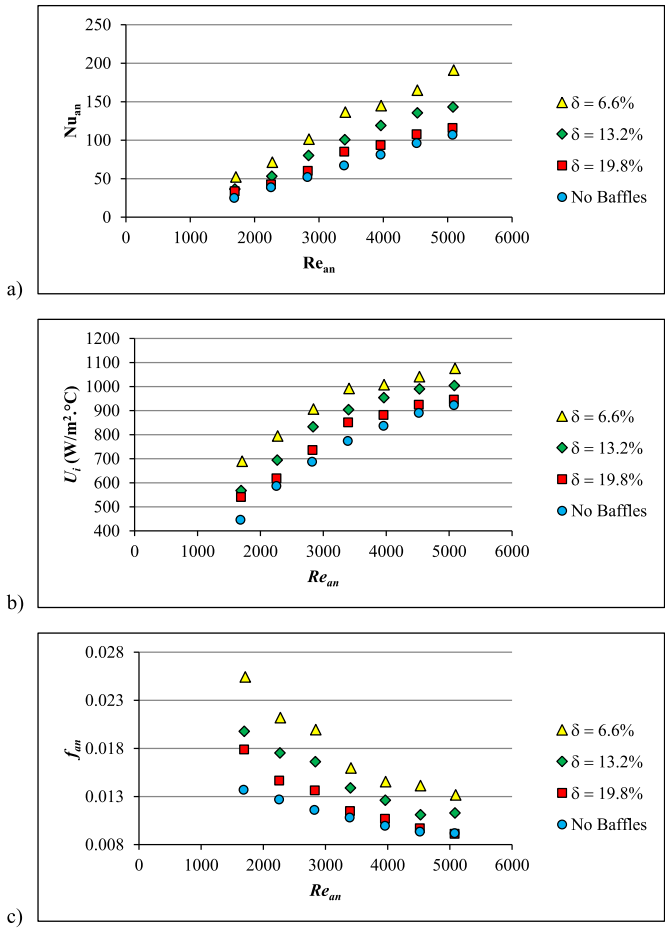

Fig. 8. Influence of SSPBs cut ratio at different annulus Reynolds numbers; (a) $\overline{Nu}_{an}$, (b) U_i, (c) f_{an}.

the corresponding number of the inserted SSPBs is 7, 5, 3 baffles.

From Fig. 9, it is obvious that decreasing λ increases $\overline{Nu}_{an}$, U_i and f_{an}. Compared with no baffles for all studied annulus-side operating conditions, the average increase in the annulus-average Nusselt number is of 10.2%–81.5%, and the average increase in the overall heat transfer coefficient is of 4.4%–26.8% and the average increase in the annulus-side friction factor is of 10.8%–63.1% when λ decreases from 13.16 to 6.58%. This is due to decreasing λ increases the chance of turbulence for the annulus flow and produces better impingement as a result of increasing number of baffles that creates a significant enhancement of heat transfer in addition to significant increase in the pressure drop.

7.5. Influence of SSPBs inclination angle

In this analysis, also four heat exchangers (SSPBs no. 1, 11, 3 and 12) are considered. Five SSPBs are inserted in the baffled heat exchangers with same holes spacing ratio ($\Psi = 2.5$), same void ratio ($\phi = 12.14\%$), same pitch ratio ($\lambda = 8.77$), same cut ratio ($\delta = 13.2\%$) while inclination angle ranges from 45° to 90°. The direction of annulus-side flow and inclined SSPBs directions are illustrated in Fig. 10.

From Fig. 11, it is noticeable that increasing θ increases $\overline{Nu}_{an}$, U_i and f_{an}. Compared with no baffles for all studied annulus-side operating conditions, the average increase in the annulus-average Nusselt number is of 20.5%–45.1%, and the average increase in the overall heat transfer coefficient is of 8.6%–17.5% and the average increase in the annulus-side friction factor is of 19%–31.8% when θ increases from 45° to 90°. This is due to increasing θ increases fluid impingement.

7.6. Influence of annulus-side operating conditions

In this analysis, the effect of annulus-side operating conditions on the thermal performance of the studied heat exchangers is presented. It is obvious from Figs. 6–9, 11 and 12 that increasing Re_{an} increases both $\overline{Nu}_{an}$ and U_i. This can be backed to increasing the fluctuations level and fluid layers mixing around the internal tube by increasing Reynolds number. On contrary, increasing Re_{an} decreases f_{an}, which can returned to that momentum forces overcomes viscous forces as Re_{an} increases.

For the effect of annulus-side inlet temperature, the results are presented here in Fig. 12 for the heat exchanger of SSPB no. (3), as a model of the results. It is evident that increasing annulus fluid inlet temperature leads to a slight decrease in both $\overline{Nu}_{an}$ and U_i. This can be attributed to decreasing Prandtl number with increasing fluid temperature. While the effect of $T_{an,\,i}$ on the annulus side friction factor is nearly negligible. This is due to lower effect of viscosity variation compared with the inertia force.

8. Thermal performance index

To be a successful heat transfer enhancement tool, the rise in convective heat transfer given due to existing perforated baffles in

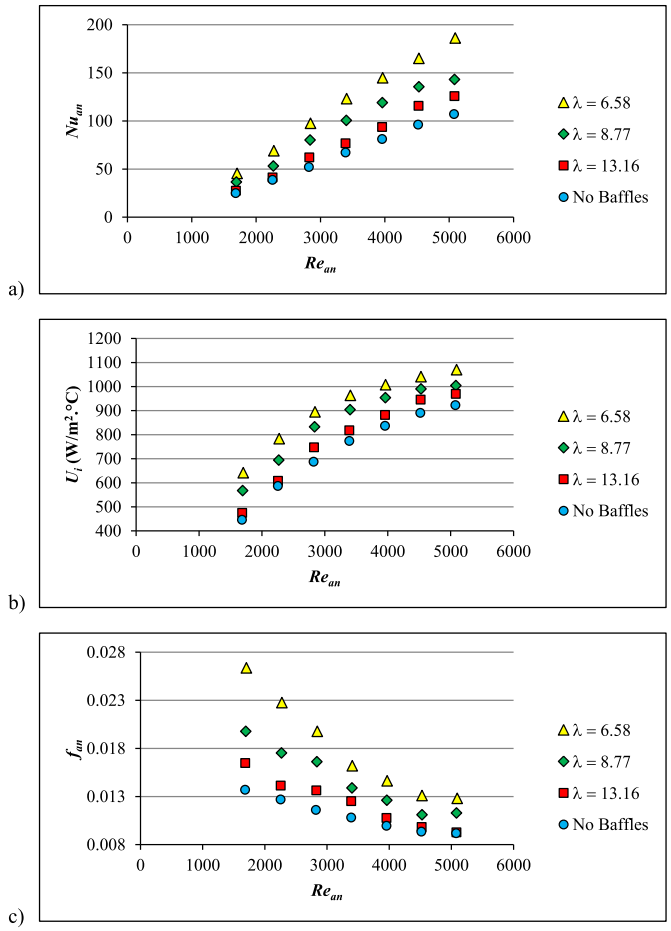

Fig. 9. Influence of SSPBs pitch ratio at different annulus Reynolds numbers; (a) $\overline{Nu}_{an}$, (b) U_i, (c) f_{an}.

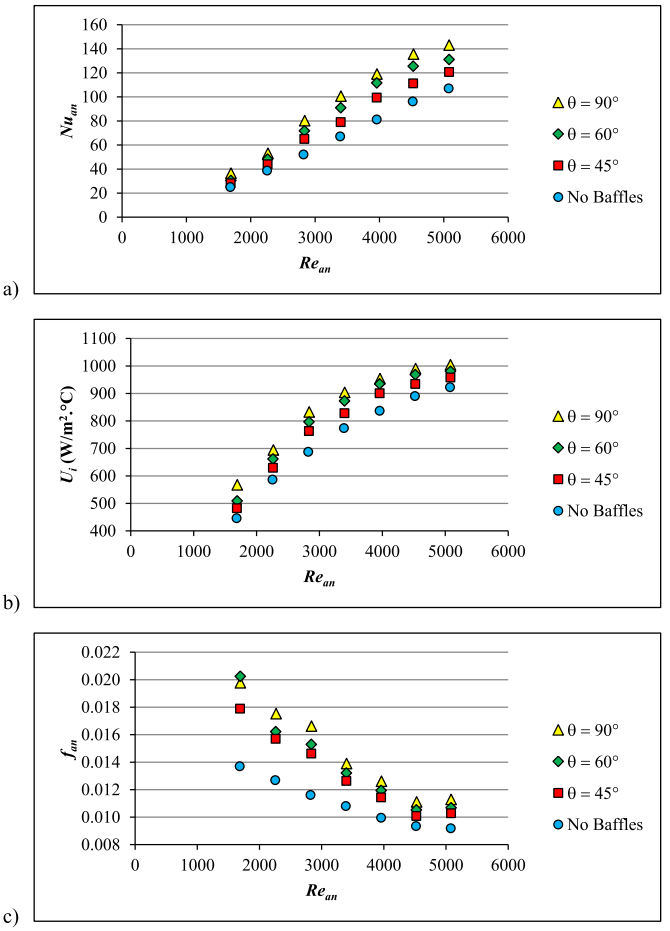

Fig. 11. Influence of SSPBs inclination angle at different annulus Reynolds numbers; (a) $\overline{Nu}_{an}$, (b) U_i, (c) f_{an}.

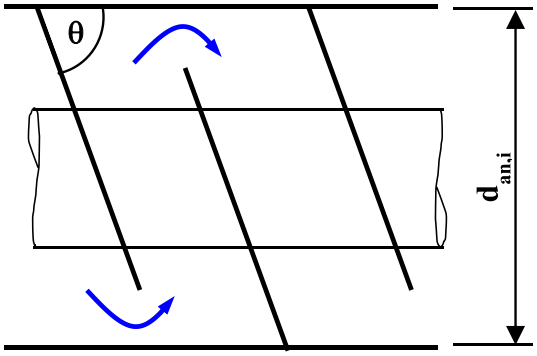

Fig. 10. Representation of annulus-side flow and inclined SSPBS directions.

heat exchangers should be higher than the rise in the fluid pressure drop at same pumping power. The thermal performance index (*TPI*) is determined using $\overline{Nu}_{an}$ ratio and f_{an} ratios [41–44] that are calculated using the values obtained for existing perforated baffles and no baffles, as follows;

$$TPI = \frac{\overline{Nu}_{an,\ baffles} \Big/ \overline{Nu}_{an,\ no\ baffles}}{\left(f_{an,\ baffles} \Big/ f_{an,\ no\ baffles}\right)^{1/3}} \tag{18}$$

Over the studied range of annulus-operating conditions, the average TPI is calculated and the results are illustrated at different SSPBs geometrical parameters in Fig. 13 for different perforated baffles characteristics. It is obvious from Fig. 13 that the TPI is more than unity for all ranges of tested perforated baffles. It increases with increasing Ψ and θ, and decreasing of ϕ, δ and λ. Over the studied range of operating conditions, the average value of TPI is of 1.62 and 1.82 at Ψ = 2 and Ψ = 3, respectively. Its values are 1.82 and 1.67 at ϕ = 6.72% and ϕ = 20.4%, respectively. In addition, its values are 2.16 and 1.46 at δ = 6.6% and δ = 19.8%, respectively. Moreover, its values are 2.01 and 1.38 at λ = 6.88% and λ = 13.16%, respectively. Furthermore, its values are 1.14 and 1.23 at θ = 45° and θ = 90°, respectively. Fig. 14 reveals a comparison for the TPI of the double pipe heat exchanger with SSPB 9, which provides the maximum TPI; 2.16, with that obtained by other recent researchers using other enhancement techniques. It is clearly shown that the present passive technique; SSPB, gives a remarkable enhancement in the thermal performance compared with other works.

9. Correlations for annulus average Nusselt numbers and friction factor

Using the present experimental data, correlations are developed through power regression models to predict the annulus average Nusselt number and its Fanning friction factor with using SSPBs inside. The annulus average Nusselt number is correlated as a function of annulus-side Reynolds and Prandtl numbers, baffles spacing ratio, void ratio, cut ratio, pitch ratio and inclination angle

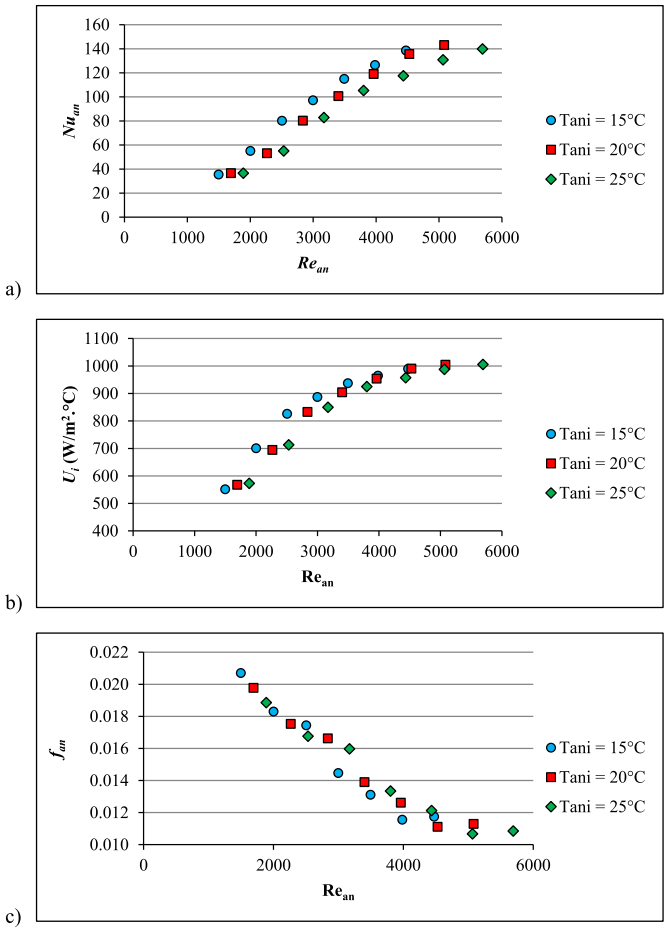

Fig. 12. Effect of annulus-side inlet temperature on the thermal performance of SSPB no. 3; (a) $\overline{Nu}_{an}$, (b) U_i, (c) f_{an}.

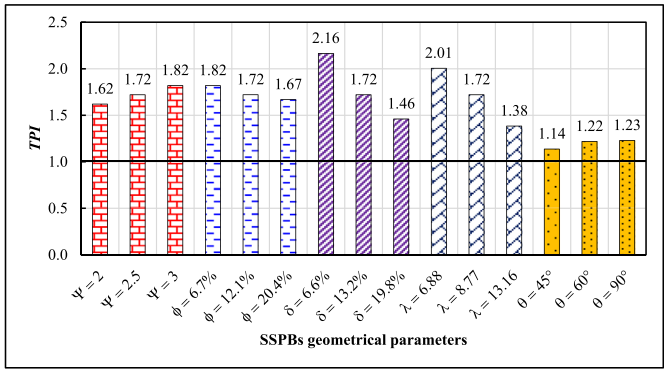

Fig. 13. Variation of thermal performance index with SSPBs geometrical parameters.

in degrees as follows;

$$\overline{Nu}_{an} = 0.0015\, Re_{an}^{1.25}\, Pr_{an}^{1.03}\, \Psi^{0.35}\, \phi^{0.31}\, \delta^{-0.46}\, \lambda^{-0.77} \left(\frac{\theta}{90}\right)^{0.21} \quad (19)$$

Additionally, a correlation for annulus-side Fanning friction factor is obtained as follows;

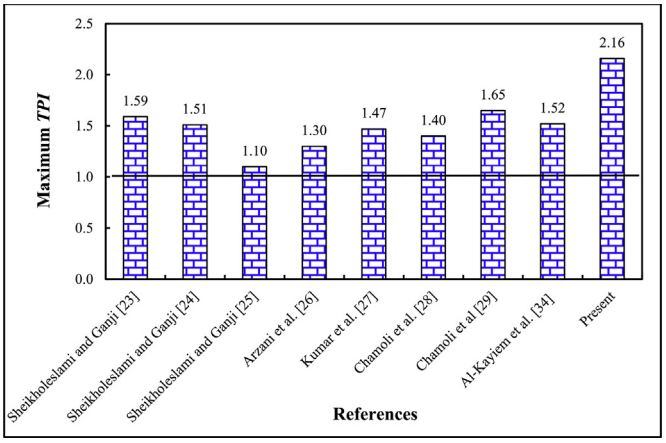

Fig. 14. Comparison of the present *TPI* with other works.

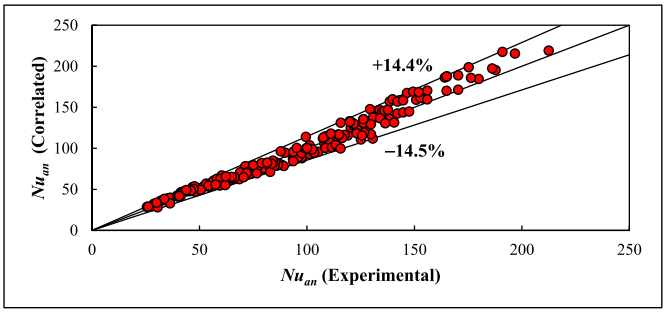

Fig. 15. Comparison of experimental values for annulus-average Nusselt number with that correlated by Eq. (19).

$$f_{an} = 3.3\, Re_{an}^{-0.58}\, \Psi^{0.22}\, \phi^{0.22}\, \delta^{-0.3}\, \lambda^{-0.5} \left(\frac{\theta}{90}\right)^{0.17} \quad (20)$$

Eqs. (19) and (20) are with correlation coefficients (R^2) of 0.997 and 0.995, respectively, and are applicable for $1380 \le Re_{an} \le 5700$, $5.82 \le Pr_{an} \le 7.86$, $2 \le \Psi \le 3$, $6.72\% \le \phi \le 20.4\%$, $6.6\% \le \delta \le 19.8\%$, $6.58\% \le \lambda \le 13.16\%$, and $45° \le \theta \le 90°$. Comparisons of the experimental annulus average Nusselt number and annulus-friction factor with those calculated by the proposed correlations are shown in Figs. 15 and 16. From these figures, it is evident that the proposed correlations are in good agreement with the present experimental data. It is clearly seen that the data falls of the proposed equations within a maximum deviation of ±14.5% and ±12.5% for $\overline{Nu}_{an}$ and f_{an}, respectively.

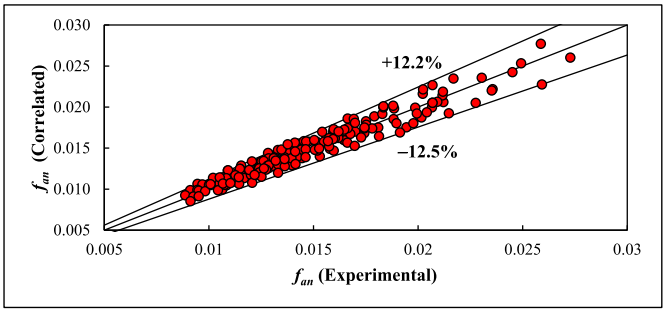

Fig. 16. Comparison of experimental values for HCT-Fanning friction factor with that correlated by Eq. (20).

10. Conclusions

The present work is carried out to investigate experimentally the heat transfer characteristics and the pressure drop in the annulus of concentric tube heat exchangers with SSPBs. The SSPB-geometrical parameters and operating conditions of the annulus side are the main parameters throughout this study. Therefore, eleven baffled heat exchangers of counter-flow configuration are constructed with different SSPBs geometries and tested at different water flow rates and inlet temperatures. In experiments, the investigated operating parameters are $1380 \le Re_{an} \le 5700$, $5.82 \le Pr_{an} \le 7.86$, $2 \le \Psi \le 3$, $6.72\% \le \phi \le 20.4\%$, $6.6\% \le \delta \le 19.8\%$, $6.58\% \le \lambda \le 13.16\%$, and $45^\circ \le \theta \le 90^\circ$.

From the previous sections and according to the results obtained using the experimental investigation, the following conclusions can be expressed:

- Installing segmental perforated baffles inside double pipe heat exchangers increases the heat transfer rate in addition to the pressure drop in the annulus side when compared with that in un-baffled heat exchangers
- The annulus average Nusselt number and friction factor increase with increasing SSPBs holes spacing ratio, void ratio and inclination angle, and with decreasing SSPBs cut ratio and pitch ratio.
- There is a slight increase in annulus average Nusselt number with decreasing the annulus-fluid inlet temperature, while its effect on the annulus side friction factor can be neglected.
- Increasing SSPBs holes spacing ratio and inclination angle, and decreasing SSPBs void ratio, cut ratio and pitch ratio enhances the thermal performance index.
- Correlations for the average Nusselt numbers in addition to the Fanning friction factor for the annulus side of the concentric tube heat exchangers with SSPBs as a function of the investigated parameters are obtained.

Appendix A

In the present study the root sum square combination of the effects of each of individual inputs as introduced by Kline and McClintock [38] are applied to determine the uncertainty in all parameters as;

$$\omega_{d_{an,\,h}} = \pm\sqrt{\left(\frac{\partial d_{an,\,h}}{\partial d_{an,\,i}}\omega_{d_{an,\,i}}\right)^2 + \left(\frac{\partial d_{an,\,h}}{\partial d_{t,\,o}}\omega_{d_{t,\,o}}\right)^2} = \pm 0.55\ \text{mm} \tag{21}$$

$$\frac{\omega_\Psi}{\Psi} = \pm\sqrt{\left(\frac{\omega_S}{S}\right)^2 + \left(\frac{-\omega_{d_h}}{d_h}\right)^2} \tag{22}$$

$$\omega_\phi = \pm\sqrt{\left(\frac{\partial\phi}{\partial d_h}\omega_{d_h}\right)^2 + \left(\frac{\partial\phi}{\partial d_b}\omega_{d_b}\right)^2 + \left(\frac{\partial\phi}{\partial d_{t,\,o}}\omega_{d_{t,\,o}}\right)^2} \tag{23}$$

$$\frac{\omega_\delta}{\delta} = \pm\sqrt{\left(\frac{\omega_H}{H}\right)^2 + \left(\frac{-\omega_{d_{an,\,i}}}{d_{an,\,i}}\right)^2} \tag{24}$$

$$\frac{\omega_\lambda}{\lambda} = \pm\sqrt{\left(\frac{\omega_{p_b}}{p_b}\right)^2 + \left(\frac{-\omega_{d_{an,\,h}}}{d_{an,\,h}}\right)^2} \tag{25}$$

$$\omega_{\Delta T_{L.M}} = \pm\frac{\omega_T\sqrt{2}}{\ln\left[\frac{\Delta T_i}{\Delta T_o}\right]}\sqrt{2 - 2\Delta T_{L.M}\left(\frac{1}{\Delta T_i} + \frac{1}{\Delta T_o}\right) + \Delta T_{L.M}^2\left(\frac{1}{\Delta T_i^2} + \frac{1}{\Delta T_o^2}\right)} \pm 0.6^\circ\text{C} \tag{26}$$

$$\frac{\omega_{A_{t,\,i}}}{A_{t,\,i}} = \pm\sqrt{\left(\frac{\omega_{d_{t,\,i}}}{d_{t,\,i}}\right)^2 + \left(\frac{\omega_{L_t}}{L_t}\right)^2} = \pm\sqrt{\left(\frac{0.00005}{0.026}\right)^2 + \left(\frac{0.0005}{1.2}\right)^2} = \pm 0.2\% \tag{27}$$

$$\frac{\omega_{A_{t,o}}}{A_{t,\,o}} = \pm\sqrt{\left(\frac{\omega_{d_{t,\,o}}}{d_{t,\,o}}\right)^2 + \left(\frac{\omega_{L_t}}{L_t}\right)^2} = \pm\sqrt{\left(\frac{0.00005}{0.028}\right)^2 + \left(\frac{0.0005}{1.2}\right)^2} = \pm 0.18\% \tag{28}$$

$$\omega_{\Delta T_t} = \pm\sqrt{\left(\frac{\partial\Delta T_t}{\partial T_{t,\,i}}\omega_{T_{t,\,i}}\right)^2 + \left(\frac{\partial\Delta T_t}{\partial T_{t,\,o}}\omega_{T_{t,\,o}}\right)^2} = \pm 0.7^\circ\text{C} \tag{29}$$

$$\frac{\omega_{Q_t}}{Q_t} = \pm\sqrt{\left(\frac{\omega_{\dot m_t}}{\dot m_t}\right)^2 + \left(\frac{\omega_{Cp_t}}{Cp_t}\right)^2 + \left(\frac{\omega_{\Delta T_t}}{\Delta T_t}\right)^2} \tag{30}$$

$$\frac{\omega_{Q_{an}}}{Q_{an}} = \pm\sqrt{\left(\frac{\omega_{\dot m_{an}}}{\dot m_{an}}\right)^2 + \left(\frac{\omega_{Cp_{an}}}{Cp_{an}}\right)^2 + \left(\frac{\omega_{\Delta T_{an}}}{\Delta T_{an}}\right)^2} \tag{31}$$

$$\omega_{Q_{ave}} = \pm\frac{1}{2}\sqrt{(\omega_{Q_t})^2 + (\omega_{Q_{an}})^2} \tag{32}$$

$$\frac{\omega_{Re_t}}{Re_t} = \pm\sqrt{\left(\frac{\omega_{\dot m_t}}{\dot m_t}\right)^2 + \left(\frac{-\omega_{d_{t,i}}}{d_{t,i}}\right)^2 + \left(\frac{-\omega_{\mu_t}}{\mu_t}\right)^2} \tag{33}$$

$$\frac{\omega_{\overline{Nu}_t}}{\overline{Nu}_t} = \pm\sqrt{\left(\frac{\omega_{Re_t}}{Re_t}\right)^2 + \left(\frac{\omega_{Pr_t}}{Pr_t}\right)^2} \tag{34}$$

$$\frac{\omega_{\overline{h}_t}}{\overline{h}_t} = \pm\sqrt{\left(\frac{\omega_{\overline{Nu}_t}}{\overline{Nu}_t}\right)^2 + \left(\frac{\omega_{k_t}}{k_t}\right)^2 + \left(\frac{-\omega_{d_{t,i}}}{d_{t,i}}\right)^2} \quad (35)$$

$$\frac{\omega_{U_i}}{U_i} = \pm\sqrt{\left(\frac{\omega_{Q_{ave}}}{Q_{ave}}\right)^2 + \left(\frac{-\omega_{A_{t,\,i}}}{A_{t,\,i}}\right)^2 + \left(\frac{-\omega_{\Delta T_{LM}}}{\Delta T_{LM}}\right)^2} \quad (36)$$

$$\omega_{\overline{h}_{an}} = \pm\sqrt{\left(\frac{\partial \overline{h}_{an}}{\partial U_i}\omega_{U_i}\right)^2 + \left(\frac{\partial \overline{h}_{an}}{\partial A_{t,\,o}}\omega_{A_{t,\,o}}\right)^2 + \left(\frac{\partial \overline{h}_{an}}{\partial A_{t,\,i}}\omega_{A_{t,\,i}}\right)^2 + \left(\frac{\partial \overline{h}_{an}}{\partial \overline{h}_t}\omega_{\overline{h}_t}\right)^2} \quad (37)$$

$$\frac{\omega_{\overline{Nu}_{an}}}{\overline{Nu}_{an}} = \pm\sqrt{\left(\frac{\omega_{\overline{h}_{an}}}{\overline{h}_{an}}\right)^2 + \left(\frac{\omega_{d_{an,\,h}}}{d_{an,\,h}}\right)^2 + \left(\frac{-\omega_{k_{an}}}{k_{an}}\right)^2} \quad (38)$$

$$\frac{\omega_{Re_{an}}}{Re_{an}} = \pm\sqrt{\left(\frac{\omega_{\dot{m}_{an}}}{\dot{m}_{an}}\right)^2 + \left(\frac{-\omega_{d_{an,\,h}}}{d_{an,\,h}}\right)^2 + \left(\frac{-\omega_{\mu_{an}}}{\mu_{an}}\right)^2} \quad (39)$$

$$\frac{\omega_{f_{an}}}{f_{an}} = \pm\sqrt{\left(\frac{\omega_{\Delta P_{an}}}{\Delta P_{an}}\right)^2 + \left(\frac{\omega_{d_{an,\,h}}}{d_{an,\,h}}\right)^2 + \left(\frac{-\omega_{L_{an}}}{L_{an}}\right)^2 + \left(\frac{-\omega_{\rho_{an}}}{\rho_{an}}\right)^2 + \left(\frac{-2\omega_{u_{an}}}{u_{an}}\right)^2} \quad (40)$$

$$\omega_{u_{an}} = \pm\sqrt{\left(\frac{\partial u_{an}}{\partial \dot{V}_{an}}\omega_{\dot{V}_{an}}\right)^2 + \left(\frac{\partial u_{an}}{\partial d_{an,\,i}}\omega_{d_{an,\,i}}\right)^2 + \left(\frac{\partial u_{an}}{\partial d_{t,\,o}}\omega_{d_{t,\,o}}\right)^2} \quad (41)$$

References

[1] Bejan Adrian, Kraus Allan D. Heat transfer handbook, vol. 1. John Wiley & Sons; 2003. p. 1030.
[2] Mehrabian MA, Hemmat M. The overall heat transfer characteristics of a double pipe heat exchanger: comparison of experimental data with predictions of standard, transactions on modelling and simulation, vol 30. WIT Press; 2001. www.witpress.com. ISSN 1743–355X.
[3] Abu-Mulaweh HI. Experimental comparison between heat transfer enhancement methods in heat exchangers. Int J Mech Eng Educ 2003;31(2):160–7.
[4] Dewan A, Mahanta P, Sumithra Raju K, Suresh Kumar P. Review of passive heat transfer augmentation techniques. Proc Instn Mech Engrs 2004;218. Part A: J. Power and Energy, A04804 © IMechE.
[5] Ganorkar AB, Kriplani VM. Review of heat transfer enhancement in different types of extended surfaces. Int J Eng Sci Technol (IJEST) 2011;3(4):3304–13.
[6] Mahureand AN, Kriplani VM. Review of heat transfer enhancement techniques. Int J Eng Res Technol 2012;5(3):241–9.
[7] Ko Kang-Hoon, Anand NK. Use of porous baffles to enhance heat transfer in a rectangular channel. Int J Heat Mass Transf 2003;46:4191–9.
[8] Yang Yue-Tzu, Hwang Chih-Zong. Calculation of turbulent flow and heat transfer in a Porous-baffled channel. Int J Heat Mass Transf 2003;46:771–80.
[9] Dutta Prashanta, Hossain Akram. Internal cooling augmentation in rectangular channel using two inclined baffles. Int J Heat Fluid Flow 2005;26:223–32.
[10] Karwa Rajendra, Maheshwari BK, Karwa Nitin. Experimental study of heat transfer enhancement in an asymmetrically heated rectangular duct with perforated baffles. Int Commun Heat Mass Transf 2005;32:275–84.
[11] Balikowski JR, Mollendorf JC. Performance of phase change materials in a horizontal annulus of a double-pipe heat exchanger in a water-circulating loop. J Heat Transf 2007;129:265–72.
[12] Targui N, Kahalerras H. Analysis of fluid flow and heat transfer in a double pipe heat exchanger with porous structures. Energy Convers Manag 2008;49:3217–29.
[13] Nasiri M, Etemad S Gh, Bagheri R. Experimental heat transfer of nanofluid through an annular duct. Int Commun Heat Mass Transf 2011;38:958–63.
[14] Ary BKP, Lee MS, Ahn SW, Lee DH. The effect of the inclined perforated baffle on heat transfer and flow patterns in the channel. Int Commun Heat Mass Transf 2012;39:1578–83.
[15] Targui N, Kahalerras H. Analysis of a double pipe heat exchanger performance by use of porous baffles and pulsating flow. Energy Convers Manag 2013;76:43–54.
[16] Chamoli Sunil, Thakur Narendra. Performance study of solar air heater duct having absorber Plate with V down perforated baffles. Songklanakarin J Sci Technol 2014;36(2):201–8.
[17] Chamoli Sunil, Singh Thakur Narender. Numerical based heat transfer and friction factor correlations of rectangular ducts roughened with transverse perforated baffles. Walailak J Sci Technol 2014;11(2):107–27.
[18] Sheikholeslami M, Gorji-Bandpy M, Ganji DD. Experimental study of the influence of perforated circular-ring on pressure loss and heat transfer enhancement using sensitivity analysis. Appl Therm Eng 2015;91:739–48.
[19] Sheikholeslami M, Gorji-Bandpy M, Ganji DD. Experimental study on turbulent flow and heat transfer in an air to water heat exchanger using perforated circular-ring. Exp Therm Fluid Sci 2016;70:185–95.
[20] Sahel Djamel, Ameur Houari, Benzeguir Redouane, Kamla Youcef. Enhancement of heat transfer in a rectangular channel with perforated baffles. Appl Therm Eng 2016;101:156–64.
[21] Kumar Anil, Kim Man-Hoe. Thermal hydraulic performance in a solar air heater channel with multi V-Type perforated baffles. Energies 2016;9(7):564.
[22] El-Maghlany Wael M, Hanafy Ahmed A, Hassan Amr A, ElMagid Mohamed A. Experimental study of Cu-Water nanofluid heat transfer and pressure drop in a horizontal double-tube heat exchanger. Exp Therm Fluid Sci 2016;78:100–11.
[23] Sheikholeslami M, Ganji DD. Heat transfer improvement in a double pipe heat exchanger by means of perforated turbulators. Energy Convers Manag 2016;127:112–23.
[24] Sheikholeslami M, Ganji DD. Heat transfer enhancement in an air to water heat exchanger with discontinuous helical turbulators; experimental and numerical studies. Energy 2016;116:341–52.
[25] Sheikholeslami Mohsen, Ganji Davood Domiri. Turbulent heat transfer enhancement in an air-to-water heat exchanger. Proceedings of the Institution of Mechanical Engineers Part E J Process Mech Eng 2016;0(0):1–14. http://dx.doi.org/10.1177/0954408916664758.
[26] Arzani Hamed Khajeh, Amiri Ahmad, Kazi SN, Chew BT, Badarudin A. Experimental investigation of thermophysical properties and heat transfer rate of covalently functionalized MWCNT in an annular heat exchanger. Int Commun Heat Mass Transf 2016;75:67–77.
[27] Kumar Alok, Chamoli Sunil, Kumar Manoj, Singh Satyendra. Experimental investigation on thermal performance and fluid flow characteristics in circular cylindrical tube with circular perforated ring inserts. Exp Therm Fluid Sci 2016;79:168–74.
[28] Chamoli Sunil, Yu Peng, Kumar Alok. Multi-response optimization of geometric and flow Parameters in A Heat exchanger tube with perforated disk inserts by Taguchi grey relational analysis. Appl Therm Eng 2016;103:1339–50.

[29] Chamoli Sunil, Lu Ruixin, Yu Peng. Thermal characteristic of a turbulent flow through a circular tube fitted with perforated vortex generator inserts. Appl Therm Eng 2017;121:1117–34.
[30] Chamoli Sunil, Yu Peng, Yu Shimin. Multi-objective shape optimization of a heat exchanger tube fitted with compound inserts. Appl Therm Eng 2017;117:708–24.
[31] Sheikholeslami M, Bhatti MM. Forced convection of nanofluid in presence of constant magnetic field considering shape effects of nanoparticles. Int J Heat Mass Transf 2017;111:1039–49.
[32] Sheikholeslami M, Shehzad SA. Magnetohydrodynamic nanofluid convection in a porous enclosure considering heat flux boundary condition. Int J Heat Mass Transf 2017;106:1261–9.
[33] Sheikholeslami Mohsen. Magnetohydrodynamic nanofluid forced convection in a porous lid driven cubic cavity using lattice Boltzmann method. J Mol Liq 2017;231:555–65.
[34] Al-Kayiem Hussain H, Ekhwan Alzakri Bin, Muhi Laheeb N. Augmentation of ribs turbulators height on the hydrothermal performance of double pipe heat exchanger. J Eng Sci Technol 2017;12(2):548–63.
[35] El Maakoul Anas, Laknizi Azzeddine, Saadeddine Said, Abdellah Abdellatif Ben, Meziane Mohamed, Metoui Mustapha El. Numerical design and investigation of heat transfer enhancement and performance for an annulus with continuous helical baffles in a double-pipe heat exchanger. Energy Convers Manag 2017;133:76–86.
[36] Remsburg Ralph. Thermal design of electronic equipment, electronics handbook series. Boca Raton: CRC PRESS LLC; 2001.
[37] Dittus FW, Boelter LMK. Heat transfer in automobile radiators of the tubular type, vol. 2. University of California Publications in Engineering; 1930. p. 443461 [Lawrence, A. E].
[38] Kline SJ, McClintock FA. Describing uncertainties in single-sample experiments. Mech Eng 1953;75(1):3–8.
[39] Gnielinski V. New equations for heat and mass transfer in turbulent pipe and channel flow. Int Chem Eng 1976;16:359–68.
[40] Filonenko GK. Hydraulic resistance of pipes (hydraulischer widerstand Von rohrleitungen). Teploenergetika 1954;1(4):40–4.
[41] Salem MR, Ali RK, Sakr RY, Elshazly KM. Effect of γ–Al_2O_3/water nanofluid on heat transfer and pressure drop characteristics of shell and coil heat exchanger with different coil curvatures. J Therm Sci Eng Appl 2015;7(4). 041002, 9 pages.
[42] Elshazly KM, Sakr RY, Ali RK, Salem MR. Effect of γ–Al2O3/water nanofluid on the thermal performance of shell and coil heat exchanger with different coil torsions, heat and mass transfer. Springer; November 2016.
[43] Webb RL, Eckert ERG. Application of rough surface to heat exchanger design. Int J Heat Mass Transf 1972;15:1647–58.
[44] Kumar Anil, Kim Man-Hoe. Heat transfer and fluid flow characteristics in air duct with various V-Pattern rib roughness on the heated plate: a comparative study. Energy 2016;103:75–85.

Nomenclatures

$\overline{h}$: Average convection heat transfer coefficient, $\frac{W}{m^2}.^\circ C$
$\dot{m}$: Mass flow rate, kg/s
$\dot{V}$: Volume flow rate, m^3/s
A: Area, m^2
Cp: Specific heat, J/kg.°C
d: Diameter, m
f: Fanning friction factor
H: Window height of the segmental baffle, m
k: Thermal conductivity, $\frac{W}{m}.^\circ C$
L: Length, m
m: Mass, kg
N: Number of baffles/holes
P: Pressure, Pa
p: Pitch of baffles, m
Q: Heat transfer rate, W
S: Spacing of perforated baffle holes, m
T: Temperature, °C
t: Time, s
U: Overall heat transfer coefficient, $\frac{W}{m^2}.^\circ C$
u: Axial velocity, m/s
V: Volume, m^3

Dimensionless groups

$\overline{Nu}$: Average Nusselt number
Nu: Nusselt number
Pr: Prandtl number
Re: Reynolds number

Greek letters

ϕ: Perforated baffle void ratio
Ψ: Perforated baffle holes spacing ratio
Δ: Differential
δ: Baffle cut ratio
θ: Baffle inclination angle, degree
λ: Baffles pitch ratio
μ: Dynamic viscosity, kg/m.s
π: Pi≡A mathematical constant≅3.1416
ρ: Density, kg/m^3
ω: Uncertainty

Superscripts and subscripts

an: Annulus
ave: Average
b: Baffle
c: Cross sectional
eq: Equivalent
f: Film
h: Hydraulic/Hole
i: Inner/inlet/internal
LM: Logarithmic Mean
m: Mean
o: Out/outer
s: Surface
t: Tube
w: Window

Acronyms and abbreviations

PVC: Polyvinyl Chloride
SSPB: Single segmental perforated baffle
TPI: Thermal performance index